Spectral investigation of the noise influencing multiqubit states

Deepak Khurana, Govind Unnikrishnan, and T. S. Mahesh[*]

Department of Physics and NMR Research Center, Indian Institute of Science Education and Research, Pune 411008, India

(Received 19 August 2016; published 27 December 2016)

Characterizing and understanding noise affecting quantum states has immense benefits in spectroscopy as well as in realizing quantum devices. Transverse relaxation times under a set of dynamical decoupling (DD) sequences with varying interpulse delays were earlier used for obtaining the noise spectral densities of single-qubit coherences. In this work, using a pair of homonuclear spins and NMR techniques, we experimentally characterize noise in certain decoherence-free subspaces. We also explore the noise of similar states in a heteronuclear spin pair. Further, using a 10-qubit system, we investigate noise profiles of various multiqubit coherences and study the scaling of noise with respect to the coherence order. Finally, using the experimentally obtained noise spectrum of the 10-qubit NOON state, we predict the performance of a Uhrig DD sequence and verify it experimentally.

I. INTRODUCTION

The inevitable presence of local or global electromagnetic noise may cause the loss of quantum coherences of spin systems or induce the redistribution of spin populations. This phenomenon, which is often described in terms of decoherence or depolarization, appears in NMR as a net relaxation of transverse or longitudinal magnetization. Combating decoherence is of utmost importance in spectroscopy and in realizing quantum devices such as quantum information processors (QIPs). Passive techniques such as decoherence-free subspaces (DFSs) [1,2] as well as active techniques such as dynamical decoupling (DD) [3] and quantum error correcting codes [4,5] have been developed to overcome decoherence. While the passive techniques rely on exploiting the symmetries in the interaction Hamiltonian, the active techniques focus on the systematic modulation of the quantum states to suppress decoherence. In the following we discuss the noise in various types of quantum coherences including DFSs, and single-quantum as well as multiple-quantum coherences.

An example of DFS is the singlet subspace in a two-qubit system [2]. In NMR, an excess population in the singlet state, over the uniformly distributed triplet states, is termed as a singlet order. It has been shown that, such an order, under favorable circumstances, has much longer lifetimes than the usual longitudinal relaxation time scales, and is therefore known as a long-lived singlet state (LLS) [6]. Similarly, the coherence between the singlet state and the zero-quantum triplet state also has longer lifetimes than the usual transverse relaxation time scales, and is therefore termed as a long-lived coherence (LLC) [7]. On the other hand, several other single- and multiple-quantum coherences lack the symmetry properties and are therefore prone to stronger decoherence [8].

In this paper we attempt to extract the noise spectra acting on various quantum coherences of NMR spin systems. Learning about the noise spectrum not only provides insights into the physical process of noise in quantum systems, but also assists in optimizing DFS conditions as well as in designing better controls for the active suppression of noise. Quantum noise spectroscopy (QNS), a tool to characterize the environmental noise, was independently proposed by Yuge *et al.* [9] and Àlvarez and Suter [10].

The paper is organized as follows. In the following section we describe the theoretical formalism of QNS. In Sec. III, we apply QNS and experimentally extract the noise spectra of some interesting quantum coherences. Finally, we conclude in Sec. IV.

II. THEORY AND METHODS

Here, we review the theoretical aspects of characterizing the noise using a single two-level quantum system (qubit) as a probe. We consider the qubit to be coupled to a bath via a purely dephasing interaction. Assuming the system Hamiltonian $\mathcal{H}_S = \omega_0 \sigma_z/2$ and the bath Hamiltonian $\mathcal{H}_B$, the joint evolution is described by the Hamiltonian

$$\mathcal{H} = \mathcal{H}_S + \mathcal{H}_{SB} + \mathcal{H}_B. \tag{1}$$

Here, $\mathcal{H}_{SB} = j_{SB}\sigma_z B/2$ describes the system-bath interaction with B being the bath operator and j_{SB} being the system-bath coupling strength. In the interaction picture of the bath Hamiltonian, the bath operator

$$B'(t) = e^{-i\mathcal{H}_B t} B e^{i\mathcal{H}_B t} \tag{2}$$

becomes time dependent. After tracing out the bath variables, the interaction Hamiltonian reduces to

$$\mathcal{H}'_{S(B)} = j_{SB} b'(t) \sigma_z/2, \tag{3}$$

where $b'(t)$ is a stochastic function. We treat the bath to be classical and $b'(t)$ to be a zero-mean stationary Gaussian process, as has been assumed before [9,10]. However, an extension to a non-Gaussian case has also been reported recently [11].

Suppose a DD sequence involving a series of π pules is applied to refocus the dephasing caused by $\mathcal{H}'_{S(B)}$. In the interaction representation associated with the DD sequence, the Hamiltonian $\mathcal{H}'_{S(B)}$ transforms to

$$\mathcal{H}''_{S(B)} = f(t) j_{SB} b'(t) \sigma_z/2, \tag{4}$$

where $f(t)$ is the modulation function that switches between $+1$ and -1 with the application of every π pulse (see Fig. 1). The Fourier transform of $f(t)$ is known as the filter function $F(\omega, \tau_f)$, where τ_f is the period of $f(t)$.
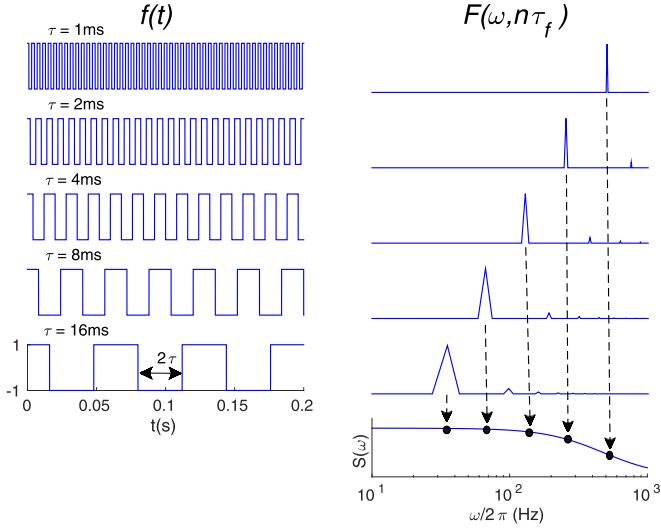
———
[*]mahesh.ts@iiserpune.ac.in

FIG. 1. The modulation functions $f(t)$ (left column) and the corresponding Fourier transforms, i.e., filter functions $F(\omega, n\tau_f)$ (right column). The first-order sampling points of the filter functions are illustrated using a schematic spectral density function $S(\omega)$ as shown in the lowest trace of the right column.

Noise spectral density $S(\omega)$ is defined as the Fourier transform of the autocorrelation function $g(\tau) = \langle b'(\tau)b'(t+\tau)\rangle$. The decay of quantum coherence is influenced by the noise spectral density as well as the filter function [12,13]. This decay can be modeled in the form $\exp[-tR(t)]$, wherein the time-dependent argument for n iterations of a DD sequence is given by

$$tR(t) = \sqrt{\frac{\pi}{2}} \int_{-\infty}^{\infty} d\omega S(\omega) |F(\omega, n\tau_f)|^2 \qquad (5)$$

[14–16].

A Fourier analysis of DD-induced modulations is similar to that of a diffraction grating. For time scales much larger than the noise correlation times, i.e., for large n, the filter function becomes time independent and reduces to a delta comb

$$|F(\omega, n\tau_f)|^2 = \sum_{k=-\infty}^{\infty} \frac{n\sqrt{2\pi}}{\tau_f} \delta(\omega - \omega_k) |F(\omega, \tau_f)|^2, \qquad (6)$$

where $\omega_k = 2\pi k/\tau_f$ and $k \in [-\infty, \infty]$ is the Fourier index of $f(t)$ [17]. The exponential decay factor now becomes time independent, i.e., $R = 1/T_2$. Hence, for a long time point $t = n\tau_f$,

$$\frac{1}{T_2} = \frac{2\pi}{\tau_f^2} \sum_{k=0}^{\infty} S(\omega_k) |F(\omega_k, \tau_f)|^2$$

$$= \sum_{k=0}^{\infty} S(\omega_k) A_k^2, \qquad (7)$$

where $A_k^2 = \frac{2\pi}{\tau_f^2} |F(\omega_k, \tau_f)|^2$ [10].

In the case of a free evolution without any DD sequence, the modulation function $f(t)$ becomes constant and therefore the filter function $F(\omega, \tau_f)$ is a sinc function centered at $\omega = 0$, and the decay rate $1/T_2$ depends only on $S(0)$.

For the Carr-Purcell-Meiboom-Gill (CPMG) sequence [18,19] with uniformly distributed π pulses at an interval 2τ, $f(t)$ switches between $+1$ and -1 with a period $\tau_f = 4\tau$. The schematic diagrams of $f(t)$ and the corresponding filter functions $|F(\omega, \tau_f)|^2$ for a set of τ values are shown in Fig. 1. In this case, $A_k^2 = (4/\pi^2 k^2)$ for odd k and $A_k = 0$ otherwise. Hence,

$$\frac{1}{T_2} = \frac{4}{\pi^2} \sum_{l=0}^{\infty} \frac{1}{(2l+1)^2} S(\omega_{2l+1}). \qquad (8)$$

Thus the decay rate $1/T_2$ for a given τ is determined by the harmonics at $\omega_{2l+1} = \pi(2l+1)/2\tau$, as illustrated in Fig. 1. Hence, from the experimentally measured T_2 values for $\tau \in [\tau_{\min}, \tau_{\max}]$, one can extract the spectral density points $S(\omega_{2l+1})$ in the range $\omega \in [\pi/2\tau_{\max}, \pi/2\tau_{\min}]$ by inverting the above equation. In the following we discuss two ways of extracting the noise spectrum $S(\omega)$ from Eq. (8).

An approximate way is to truncate the series in Eq. (8) to the zeroth-order term so that

$$S\left(\frac{\pi}{2\tau}\right) \approx \frac{\pi^2}{4T_2}. \qquad (9)$$

This method is suitable for spectral densities with sharp cutoffs at low frequencies [20]. Otherwise, ignoring higher-order terms may introduce an error up to about 10%.

On the other hand, we can account for the zeroth- as well as many higher-order terms of spectral density by using a suitable model function for the spectral density. Random isotropic rotations of liquid molecules usually lead to exponential autocorrelation function and therefore the corresponding spectral density is Lorentzian [12]. Multiple relaxation sources may lead to a multi-Lorentzian spectral density as observed in the experiments described in the next section. Our phenomenological model thus consists of a linear combination of Lorentzians

$$S_L(\omega) = \sum_{j=1}^{L} \frac{\lambda_j}{(\omega - \omega_j)^2 + \lambda_j^2}. \qquad (10)$$

The parameters ω_j (center frequency) and λ_j (linewidth) can be determined by numerically maximizing the overlap between the experimental T_2 values and those calculated using the model function $S_L(\omega)$. Another benefit of obtaining the functional form of the spectral density is that it allows one to evaluate the performance of various DD sequences at arbitrary interpulse spacing, as illustrated in Sec. III C.

Although noise filtering techniques for multiqubit states are currently being developed [21,22], in this work we use a single-probe qubit to capture the effective noise influencing multiqubit states.

III. EXPERIMENTS AND RESULTS

In this section, we describe the experimental noise spectroscopy of certain interesting multiqubit coherences.

A. LLS and LLC

We used the two phenyl ^{1}H nuclei of 2,3,6-trichlorophenol dissolved in dimethyl sulfoxide-D6 (DMSO). The experiments
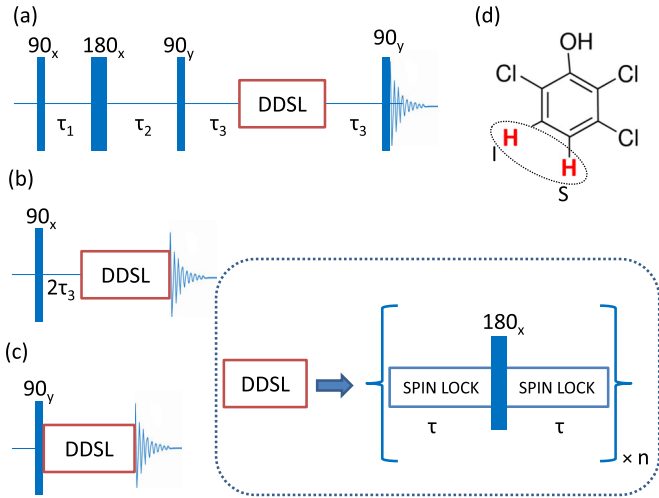
FIG. 2. Pulse sequences used to measure the noise spectrum of (a) ρ_{LLS}, (b) ρ_{LLC}, and (c) ρ_{SL}. Here, $\tau_1 = 1/(4J)$, $\tau_2 = 1/(4J) + 1/(2\Delta\nu)$, $\tau_3 = 1/(4\Delta\nu)$, and n is the number of times the loop is repeated. (d) Structure of 2,3,6-trichlorophenol. The CPMG DD sequence with spin lock along the x axis is shown in the inset (DDSL).

were carried out at 300 K in two different magnetic fields corresponding to Larmor frequencies $\nu_0 = 400\,\text{MHz}$ as well as $\nu_0 = 600\,\text{MHz}$. The chemical shift difference $\Delta\nu \times 10^6/\nu_0 = 0.21$ ppm and the scalar coupling constant $J = 8$ Hz. Under a weak-coupling approximation, the NMR Hamiltonian is

$$\mathcal{H} = \pi\Delta\nu I_z - \pi\Delta\nu S_z + \pi J 2I_z S_z, \qquad (11)$$

where I_z and S_z are the spin operators.

The natural choice for expressing LLS and LLC is the singlet-triplet basis, formed by the eigenvectors of the isotropic interaction Hamiltonian $\mathbf{I} \cdot \mathbf{S}$, i.e.,

$$
\begin{aligned}
|T_0\rangle &= \frac{1}{\sqrt{2}}(|01\rangle + |10\rangle), \\
|T_+\rangle &= |00\rangle, \\
|T_-\rangle &= |11\rangle, \\
|S_0\rangle &= \frac{1}{\sqrt{2}}(|01\rangle - |10\rangle),
\end{aligned}
\qquad (12)
$$

where $\{|00\rangle, |01\rangle, |10\rangle, |11\rangle\}$ form the Zeeman eigenbasis.

In particular, we focus on the following coherences:

$$
\begin{aligned}
\rho_{LLS} &= |S_0\rangle\langle S_0| - |T_0\rangle\langle T_0|, \\
\rho_{LLC} &= |S_0\rangle\langle T_0| + |T_0\rangle\langle S_0|, \\
\rho_{SL} &= |T_+\rangle\langle T_+| - |T_-\rangle\langle T_-|.
\end{aligned}
\qquad (13)
$$

In the above, ρ_{LLS}, ρ_{LLC}, and ρ_{SL} are realized by preparing the states $-\mathbf{I} \cdot \mathbf{S}$, $I_x - S_x$, and $I_x + S_x$, respectively, and applying a strong spin lock along the x axis [6,7]. Here, we have considered ρ_{SL} for the sake of comparison with the other long-lived states. The pulse sequences corresponding to these states are shown in Fig. 2.

We use the multi-Lorentzian model function described in Sec. II to extract the noise spectrum. The best fit was achieved with a minimum of three Lorentzian functions (i.e., $L = 3$) as described in Eq. (10). We scan over a range of spectral
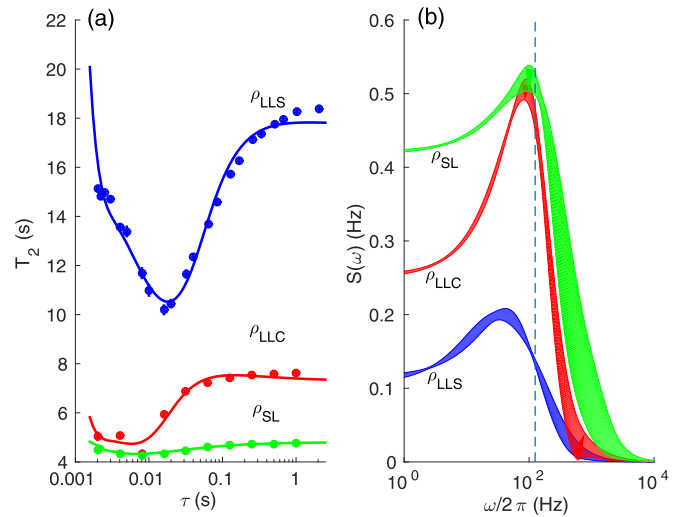

FIG. 3. (a) Experimental decay constants (dots) of 2,3,6-trichlorophenol (averaged for both protons) in a 400 MHz spectrometer for a range of τ values and for different states as indicated. The solid lines correspond to decay constants obtained from the best fit by the three-Lorentzian model as described in Eq. (10). (b) The corresponding noise spectral density bands. The dashed line at 125 Hz corresponds to the maximum harmonics sampled with $\tau = 2$ ms.

frequencies $\omega = \pi/2\tau$ by varying the duration 2τ between the π pulses, and measure the corresponding T_2 values. A WALTZ-16 spin lock of 2 kHz amplitude was applied along the x axis during the delays between the π pulses. The experimental T_2 values for all the three states and for τ values ranging from 2 ms to 2 s are displayed in Fig. 3(a). The uncertainties in the noise spectrum (represented by the width of the bands) are estimated by several iterations of maximizations also considering the standard deviations in T_2 values.

As expected, ρ_{LLS} has the lowest noise in the whole frequency range, indicating long lifetimes. On the other hand, ρ_{SL} has the highest noise, indicating a relatively short-lived state. The long-lived coherence ρ_{LLC} has an intermediate noise profile. Owing to the hardware limitations, the highest frequency sampled by the experiments is 125 Hz [indicated by a dotted line in Fig. 3(b)], corresponding $\tau = 2$ ms. The noise profiles above this cutoff frequency are basically an extrapolation obtained by the model functions. Interestingly, in all the three spectral density profiles we observe a hump close to 100 Hz. Replacing the hydroxyl proton with deuterium did not affect the hump. We have also observed a systematic dependence of the hump with the spin-lock power, which possibly relates its origin to an interference between spin-lock and DD sequences. However, further investigations are required to confirm this point.

Although it is well known that the singlet state is longer lived at lower fields [23], it is not obvious how the spectral characteristics of noise changes under a higher field. Therefore, it is useful to compare the noise spectrum at two different fields. With this intention, we have measured the noises of a singlet state of the same system, i.e., the proton pair of 2,3,6-trichlorophenol, at 400 MHz as well as at 600 MHz spectrometers under identical conditions. The T_2 values and
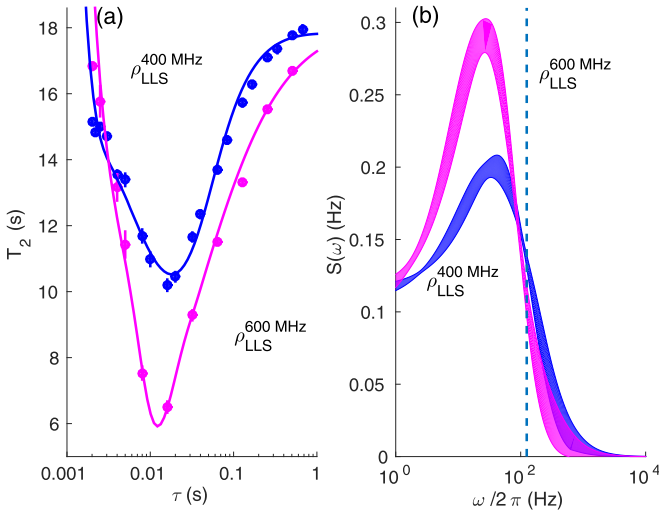
FIG. 4. (a) The experimental decay constants (dots) at various τ delays for the singlet state ρ_{LLS} at two different magnetic fields, i.e., 400 and 600 MHz, as indicated. The solid lines correspond to decay constants obtained from the best fit by the three-Lorentzian model as described in Eq. (10). (b) The corresponding noise spectra.

the corresponding spectral density bands are shown in Fig. 4. As expected, the noise is significantly stronger at 600 MHz.

B. Heteronuclear spin pair

In a hetronuclear spin pair, such as ^{1}H-^{13}C in ^{13}C chloroform [dissolved in CDCl$_3$; see Fig. 5(b)], the singlet subspace is not a DFS, because a strong magnetic field breaks the symmetry between two spins and a spin lock to restore the symmetry is not practical. Therefore, a heteronuclear singlet state, though easy to prepare, is no longer an eigenstate of the interaction Hamiltonian. A pulse sequence to measure their noise spectrum is shown in Fig. 5(a). It begins with a $\theta = \cos^{-1}(1/4)$ pulse on the ^{1}H spin followed by a pulsed-field gradient to equalize the polarizations and prepare the state $I_z + S_z$. The following rf pulses and delays convert it to $-I_x S_x - I_y S_y \equiv |S_0\rangle\langle S_0| - |T_0\rangle\langle T_0|$. A CPMG DD sequence
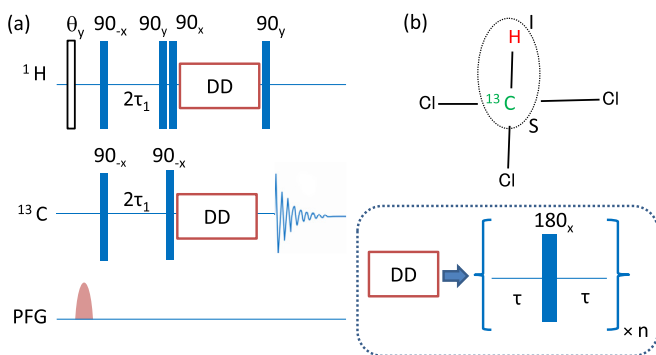

FIG. 5. (a) Pulse sequence to measure the noise spectrum in a heteronuclear spin system. (b) Molecular structure of chloroform. Here, the singlet state is prepared on ^{1}H and ^{13}C spins with a coupling constant $J_{\text{CH}} = 209$ Hz between them. The CPMG DD sequence is shown in the inset.
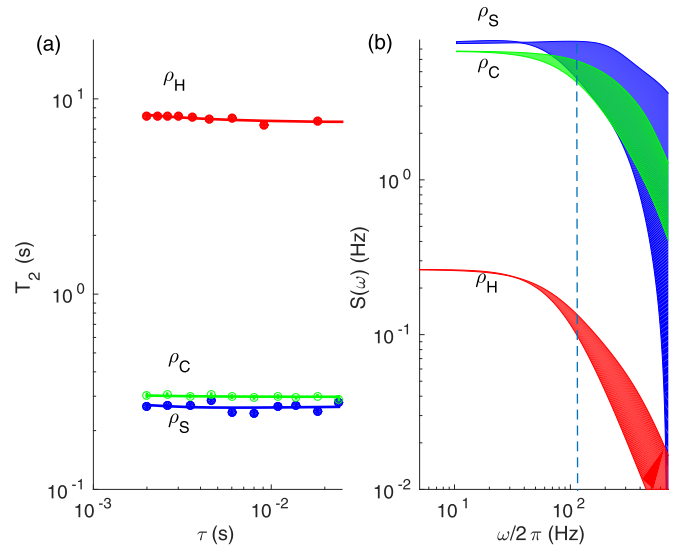

FIG. 6. (a) The experimental decay constants (dots) of ^{13}C chloroform at various τ delays for single-spin states $\rho_H = I_x$, $\rho_C = S_x$, and the singlet state ρ_S at 500 MHz. The solid lines correspond to decay constants obtained from the best fit by the three-Lorentzian model as described in Eq. (10). (b) The corresponding noise spectra.

with a variable τ delay followed by a final 90_y on ^{1}H is then used to measure the noise spectrum. The results are shown in Fig. 6. For comparison, we have also included the noise spectra of single-spin states I_x and S_x. Here ^{1}H spin has longer T_2 values and accordingly lower noise profile compared to ^{13}C. Unlike in the homonuclear case, the heteronuclear singlet has the shortest T_2 values and therefore the highest noise profile. Therefore, a heteronuclear singlet is not an LLS at high fields [24].

C. Large quantum coherences

Consider an N-spin star-topology system wherein a central spin (denoted by M) is uniformly coupled to $N-1$ magnetically equivalent spins (denoted by A). Such a system allows a convenient way to prepare many large quantum coherences. The method involves applying a Hadamard gate (denoted by H) on the central spin followed by a controlled-NOT (CNOT) gate as described in Fig. 7. In thermal equilibrium, the central spin will have an excess $|0\rangle_M$ population while the surrounding spins have a Boltzmann distribution over all the states $|N-1,0\rangle_A$ to $|0,N-1\rangle_A$, wherein the first and second numbers denote the numbers of spins in the $|0\rangle$ and $|1\rangle$ states, respectively. The effect of Hadamard and CNOT gates can now be described as

$$|0\rangle_M \sum_{k=0}^{N-1} |N-1-k,k\rangle_A$$

$$\xrightarrow{\text{H}} \frac{|0\rangle_M + |1\rangle_M}{\sqrt{2}} \sum_{k=0}^{N-1} |N-1-k,k\rangle_A$$

$$\xrightarrow{\text{CNOT}} \frac{1}{\sqrt{2}} \sum_{k=0}^{N-1} |0\rangle_M |N-1-k,k\rangle_A + |1\rangle_M |k,N-1-k\rangle_A.$$
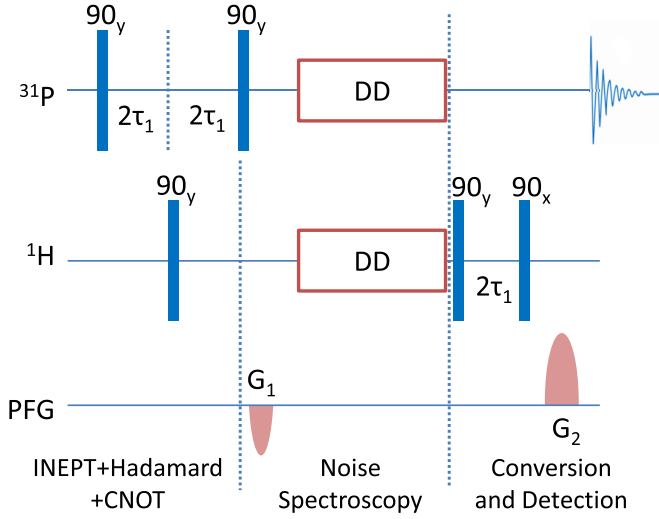
FIG. 7. Pulse sequence to measure noise spectra of the MSSM states. An initial INEPT (insensitive nuclei enhanced by polarization transfer) [25] operation is used to transfer magnetization from ^{1}H to ^{31}P. The PFGs G_1 and G_2 are chosen such that $\phi_2(k) = -\phi_1(k)$ to select out an MSSM state with a particular lopsidedness $l(k)$. A CPMG-DD sequence with composite π pulses was used.

The last sum represents a collection of coherences with quantum numbers $N, N - 2, \ldots, 0$ for even N and $N, N - 2, \ldots, 1$ for odd N. Such coherences are often referred to as |MSSM⟩ (many-some, some-many) states [8]. A special MSSM state is the N-quantum |NOON⟩ state

$$|NOON\rangle = (|000\ldots0\rangle + |111\ldots1\rangle)/\sqrt{2}. \quad (14)$$

The MSSM states can be individually studied by selective filtering of their signals using a pair of pulsed-field gradients (PFGs) (see Fig. 7). If γ_A and γ_M denote the respective gyromagnetic ratios of A and M spins, we can express the dephasing caused by the first PFG by

$$\phi_1(k) \propto \frac{\gamma_M + (N - 2k - 1)\gamma_A}{\gamma_A} = l(k), \quad (15)$$

where the term in the right-hand side is known as the lopsidedness of the MSSM state and

$$\frac{\gamma_M - (N - 1)\gamma_A}{\gamma_A} \leqslant l(k) \leqslant \frac{\gamma_M + (N - 1)\gamma_A}{\gamma_A}. \quad (16)$$

Each MSSM state is converted back into an observable single-quantum M spin coherence by the application of a second CNOT,

$$\frac{1}{\sqrt{2}} \sum_{k=0}^{N-1} |0\rangle_M |N - 1 - k, k\rangle_A + e^{i\phi_1(k)}|1\rangle_M |k, N - 1 - k\rangle_A$$

$$\xrightarrow{\text{CNOT}} \left(\sum_{k=0}^{N-1} \frac{|0\rangle_M + e^{i\phi_1(k)}|1\rangle_M}{\sqrt{2}} \right) |N - 1 - k, k\rangle_A.$$

Selection of the signal from a desired MSSM state with a particular $l(k)$ value is achieved with the help of a second PFG which introduces a phase $\phi_2(k) = -\phi_1(k)$. The noise spectroscopy of the MSSM states can be studied by inserting the DD sequence just before the second CNOT (see Fig. 7).
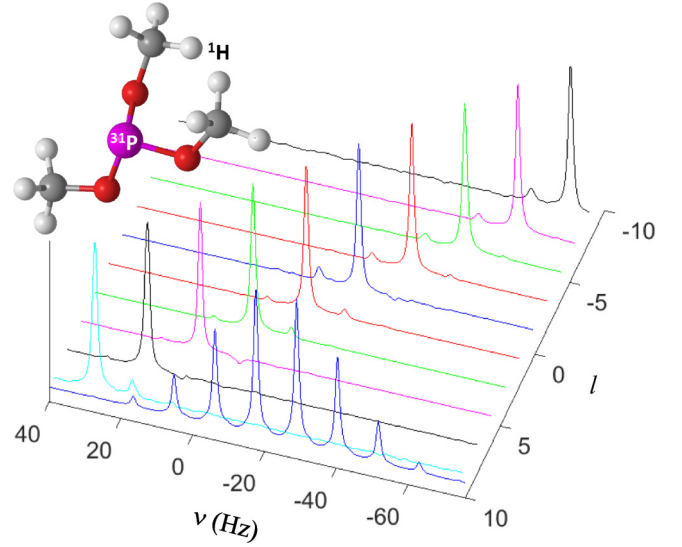

FIG. 8. The spectral lines corresponding to various MSSM states with varying lopsidedness l. Each spectral line is individually normalized. The reference spectrum with all the lines is shown at the front. The structure of trimethylphosphite is also shown at the top-left-hand corner.

Experiments were carried out in a Bruker 500 MHz spectrometer at 300 K. Trimethylphosphite (see Fig. 8) dissolved in DMSO was used as a 10-spin star-topology system including a central ^{31}P spin (M spin) and the nine surrounding ^{1}H spins (A spins). The scalar spin-spin coupling J_{PH} was about 11 Hz. The signals from various MSSM states (obtained with the pulse sequence shown in Fig. 7) along with a reference spectrum are shown in Fig. 8.

Results and discussions. The results of the noise spectroscopy of various MSSM states are shown in Fig. 9. As expected, the spectral density profiles appear to go higher with
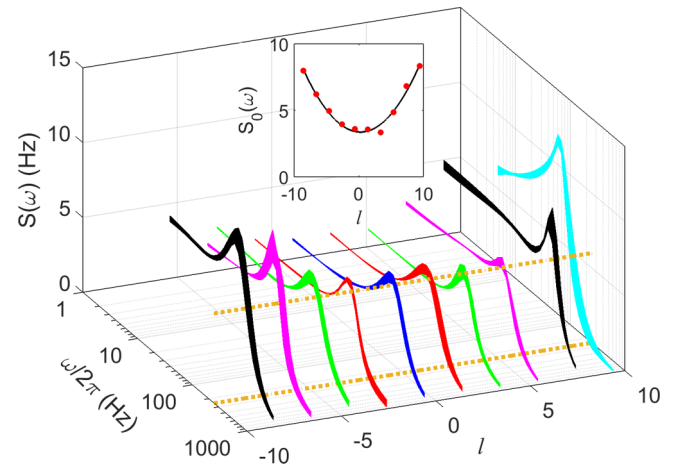

FIG. 9. Trimethylphosphite noise spectra for various MSSM states with different lopsidedness l. The dashed lines parallel to the l axis represent the maximum frequency (250 Hz) sampled in experiments. The inset shows the scaling of low-frequency spectral density values with l.

the magnitude of the lopsidedness, and accordingly the NOON state has the highest noise profile.

It is interesting to study the scaling of the low-frequency noise [$\approx S(0)$] versus the lopsidedness. The inset of Fig. 9 shows the experimental values of low-frequency noise (at the lowest frequencies sampled) and a fit with a shifted parabola $c_2 l^2 + c_0$. The best fit was found at $c_2 = 0.06 \pm 0.01$ and $c_0 = 3.37 \pm 0.34$. A quadratic scaling of noise with lopsidedness is obvious from the inset in Fig. 9.

According to Redfield theory of relaxation, the transverse relaxation is a result of two processes, adiabatic and nonadiabatic [12,26]. The energy conserving adiabatic part arises by longitudinal noise and leads to dephasing. The nonadiabatic part is due to the transverse noise and can induce transitions. Tang *et al.* had observed that the completely correlated longitudinal noise results in relaxation rates that vary quadratically with the coherence order [27]. In our system, the coherence order is characterized by lopsidedness. Thus the quadratic dependence of spectral density with lopsidedness points out that the noise is predominantly correlated, i.e., noise affects all the spins identically. The background part in the scaling (c_0) is due remaining contributions including the nonadiabatic relaxation and the self-relaxation of the probe qubit (^{31}P).

It can be noted that similar studies of scaling of decoherence were earlier reported in a solid-state NMR system by Krojanski *et al.* [28].

An immediate application of extracting the noise spectrum is in evaluating the performances of various types of DD sequences and selecting the optimum sequence for preserving quantum coherences. Uhrig dynamical decoupling (UDD) [29], for example, involves a nonuniform distribution of π pulses placed at time instants

$$t_j = \tau_c \sin^2\left(\frac{\pi j}{2N_\pi + 2}\right), \tag{17}$$

where N_π is the total number of π pulses in one period (τ_c), also known as the order of the UDD sequence (denoted UDD-N_π). It can be easily seen that UDD-1 and UDD-2 are identical to a CPMG sequence.

Having the functional form of the noise spectral density we can now predict the relative decay rates of a quantum state under a given DD sequence. As an example, the band in Fig. 10 shows the predicated decay rates of the NOON state (spectral density shown in Fig. 9) under the UDD-3 sequence for a range of τ_c values. The corresponding experimental decay rates are shown by dots. The reasonable agreement between experimental and predicted values of decay rates demonstrates the benefit of extracting the spectral distribution of noise. Similar results were obtained in the case of other MSSM states. It should be noted that imperfections in the π pulses such as finite duration, sensitivity to rf inhomogeneity over the sample volume, and calibration errors may introduce additional uncertainties in the noise-spectrum estimation and may affect DD performance as well.

IV. CONCLUSIONS

While we are entering the era of quantum devices, noise remains a hurdle in storing quantum superpositions. Exploiting
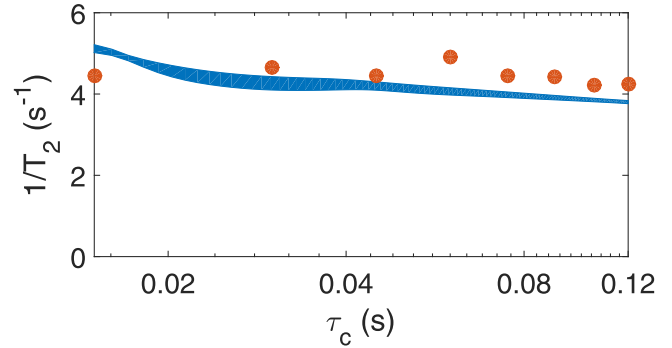

FIG. 10. Decay rates vs UDD-3 cycle duration τ_c calculated using Eq. (7) for the experimental noise spectrum of a 10-qubit NOON state. The dots correspond to experimental results.

decoherence-free subspaces (DFSs) is one of the convenient ways to preserve quantum coherences. DFS is already being used for storing hyperpolarization [30], studying slow molecular dynamics [31], characterizing molecular diffusion [32,33], precise measurements of coupling constants [34], as well as in fault-tolerant quantum computing [35]. However, the noises influencing such special quantum coherences have not been hitherto characterized experimentally. In this work we have experimentally characterized and compared noise spectral densities of various multiqubit coherences.

We found that the noise spectrum of the long-lived singlet state (LLS) under spin lock of a homonuclear spin pair had the lowest profile, indicating the strong protection offered by the symmetry in DFS resulting in long-livedness of the state. The long-lived coherence (LLC) between a singlet and the zero-quantum triplet had a higher noise profile, but still lower than the normal uncorrelated (single-spin) coherence. We have also measured the extent of noise in LLS under different field strengths and, as expected, we found a higher noise with a stronger field, although the overall spectral features remained similar. On the other hand, the uncorrelated spins showed a lower noise content compared to singlet states in a heteronuclear spin system, indicating an asymmetry in the system. Further, we have also explored the noise profiles of various higher-order coherences in a 10-spin system, and found a predominantly quadratic scaling of noise with respect to coherence order. Finally, using the noise spectrum of the NOON state, we predicted its decay rates under a third-order Uhrig dynamical decoupling sequence and verified the same with experiments.

We believe that such studies are useful for understanding the physics of noise affecting quantum systems as well as to design ways to suppress decoherence. A better understanding of noise and its suppression will be crucial not only for the physical realization of quantum devices but also for general spectroscopic applications.

[1] D. A. Lidar, I. L. Chuang, and K. B. Whaley, Decoherence-Free Subspaces for Quantum Computation, Phys. Rev. Lett. **81**, 2594 (1998).

[2] D. A. Lidar and K. B. Whaley, in *Irreversible Quantum Dynamics*, edited by F. Benatti and R. Floreanini, Lecture Notes in Physics Vol. 622 (Springer, Berlin, 2003), Pt. II, pp. 83–120.

[3] L. Viola, E. Knill, and S. Lloyd, Dynamical Decoupling of Open Quantum Systems, Phys. Rev. Lett. **82**, 2417 (1999).

[4] D. G. Cory, M. D. Price, W. Maas, E. Knill, R. Laflamme, W. H. Zurek, T. F. Havel, and S. S. Somaroo, Experimental Quantum Error Correction, Phys. Rev. Lett. **81**, 2152 (1998).

[5] J. Preskill, Reliable quantum computers, Proc. R. Soc. London, Ser. A **454**, 385 (1998).

[6] M. Carravetta and M. H. Levitt, Long-lived nuclear spin states in high-field solution NMR, J. Am. Chem. Soc. **126**, 6228 (2004).

[7] R. Sarkar, P. Ahuja, P. R. Vasos, and G. Bodenhausen, Long-Lived Coherences for Homogeneous Line Narrowing in Spectroscopy, Phys. Rev. Lett. **104**, 053001 (2010).

[8] J. A. Jones, S. D. Karlen, J. Fitzsimons, A. Ardavan, S. C. Benjamin, G. A. D. Briggs, and J. J. L. Morton, Magnetic field sensing beyond the standard quantum limit using 10-spin NOON states, Science **324**, 1166 (2009).

[9] T. Yuge, S. Sasaki, and Y. Hirayama, Measurement of the Noise Spectrum Using a Multiple-Pulse Sequence, Phys. Rev. Lett. **107**, 170504 (2011).

[10] G. A. Álvarez and D. Suter, Measuring the Spectrum of Colored Noise by Dynamical Decoupling, Phys. Rev. Lett. **107**, 230501 (2011).

[11] L. M. Norris, G. A. Paz-Silva, and L. Viola, Qubit Noise Spectroscopy for Non-Gaussian Dephasing Environments, Phys. Rev. Lett. **116**, 150503 (2016).

[12] A. Abragam, *Principles of Nuclear Magnetism*, International Series of Monographs on Physics No. 32 (Oxford University Press, Oxford, U.K., 1961).

[13] M. J. Biercuk, A. C. Doherty, and H. Uys, Dynamical decoupling sequence construction as a filter-design problem, J. Phys. B **44**, 154002 (2011).

[14] A. G. Kofman and G. Kurizki, Universal Dynamical Control of Quantum Mechanical Decay: Modulation of the Coupling to the Continuum, Phys. Rev. Lett. **87**, 270405 (2001).

[15] A. G. Kofman and G. Kurizki, Unified Theory of Dynamically Suppressed Qubit Decoherence in Thermal Baths, Phys. Rev. Lett. **93**, 130406 (2004).

[16] Ł. Cywiński, R. M. Lutchyn, C. P. Nave, and S. Das Sarma, How to enhance dephasing time in superconducting qubits, Phys. Rev. B **77**, 174509 (2008).

[17] A. Ajoy, G. A. Álvarez, and D. Suter, Optimal pulse spacing for dynamical decoupling in the presence of a purely dephasing spin bath, Phys. Rev. A **83**, 032303 (2011).

[18] H. Y. Carr and E. M. Purcell, Effects of diffusion on free precession in nuclear magnetic resonance experiments, Phys. Rev. **94**, 630 (1954).

[19] S. Meiboom and D. Gill, Modified spin-echo method for measuring nuclear relaxation times, Rev. Sci. Instrum. **29**, 688 (1958).

[20] S. S. Hegde and T. S. Mahesh, Engineered decoherence: Characterization and suppression, Phys. Rev. A **89**, 062317 (2014).

[21] Z.-K. Su and S.-J. Jiang, Filter-design perspective applied to dynamical decoupling of a multi-qubit system, J. Phys. B **45**, 025502 (2012).

[22] G. A. Paz-Silva, S.-W. Lee, T. J. Green, and L. Viola, Dynamical decoupling sequences for multi-qubit dephasing suppression and long-time quantum memory, New J. Phys. **18**, 073020 (2016).

[23] G. Pileio and M. H. Levitt, Theory of long-lived nuclear spin states in solution nuclear magnetic resonance. II. Singlet spin locking, J. Chem. Phys. **130**, 214501 (2009).

[24] M. H. Levitt, Singlet nuclear magnetic resonance, Annu. Rev. Phys. Chem. **63**, 89 (2012).

[25] J. Cavanagh, W. J. Fairbrother, A. G. Palmer III, and N. J. Skelton, *Protein NMR Spectroscopy: Principles and Practice* (Academic, New York, 1995).

[26] A. G. Redfield, The theory of relaxation processes, Adv. Magn. Opt. Reson. **1**, 1 (1965).

[27] J. Tang and A. Pines, Multiple quantum NMR and relaxation of an oriented CH_3 group, J. Chem. Phys. **72**, 3290 (1980).

[28] H. G. Krojanski and D. Suter, Scaling of Decoherence in Wide NMR Quantum Registers, Phys. Rev. Lett. **93**, 090501 (2004).

[29] G. S. Uhrig, Keeping a Quantum Bit Alive by Optimized π-Pulse Sequences, Phys. Rev. Lett. **98**, 100504 (2007).

[30] P. Ahuja, R. Sarkar, S. Jannin, P. R. Vasos, and G. Bodenhausen, Proton hyperpolarisation preserved in long-lived states, Chem. Commun. **46**, 8192 (2010).

[31] R. Sarkar, P. R. Vasos, and G. Bodenhausen, Singlet-state exchange NMR spectroscopy for the study of very slow dynamic processes, J. Am. Chem. Soc. **129**, 328 (2007).

[32] R. Sarkar, P. Ahuja, P. R. Vasos, and G. Bodenhausen, Measurement of slow diffusion coefficients of molecules with arbitrary scalar couplings via long-lived spin states, ChemPhysChem **9**, 2414 (2008).

[33] S. Cavadini, J. Dittmer, S. Antonijevic, and G. Bodenhausen, Slow diffusion by singlet state NMR spectroscopy, J. Am. Chem. Soc. **127**, 15744 (2005).

[34] A. Bornet, S. Jannin, J. A. Konter, P. Hautle, B. Van Den Brandt, and G. Bodenhausen, Ultra high-resolution NMR: Sustained induction decays of long-lived coherences, J. Am. Chem. Soc. **133**, 15644 (2011).

[35] D. Bacon, J. Kempe, D. A. Lidar, and K. B. Whaley, Universal Fault-Tolerant Quantum Computation on Decoherence-Free Subspaces, Phys. Rev. Lett. **85**, 1758 (2000).